Electronic Supplementary Material (ESI) for Dalton Transactions.
This journal is © The Royal Society of Chemistry 2019

SUPPORTING INFORMATION

Cu_4I_4- cubane clusters based on 10-(aryl)phenoxarsines and their luminescence

Milyausha F. Galimova,[a] Ekaterina M. Zueva,[a,b] Alexey B. Dobrynin,[a] Aida I. Samigullina,[a] Rustem R. Musin,[b] Elvira I. Musina,[a] and Andrey A. Karasik[a]

[a] Arbuzov Institute of Organic and Physical Chemistry, FRC Kazan Scientific Center, Russian Academy of Sciences, 8 Arbuzov Street, Kazan 420088, Russian Federation

[b] Kazan National Research Technological University, 68 Karl Marx Street, Kazan 420015, Russian Federation

Table of Contents

I. Single crystal and powder X-ray diffraction data (Tables S1–S3 and Figures S1, S2). S2

II. Photophysical properties

Experimental data (Figures S3–S15)……...…….. S5

DFT-computed data for the ligands (Figures S16–S19)……...……. S10

DFT-computed data for the complexes (Table S4, S5 and Figures S20–S21)……..……... S15

III. A collection of the solid-state phosphorescence emission maxima data for different Cu_4I_4 cubanes at room temperature (Table S6)……. S22

I. Single crystal and powder X-ray diffraction data

Table S1. Selected structural parameters (distances in Å, angles in °) for **1**, **3**, **4**, and **5**.

	Ligands				
	1	**3**	**4**	**5**	
				A	**B**
As1…*P*(C1C6C7C12)	0.281	0.196	0.293	0.342	0.388
O1…*P*(C1C6C7C12)	0.225	0.161	0.208	0.207	0.201
As1…C13	1.960	2.004	1.974	1.980	1.972
∠C13-As1-C1	99.47	98.32	99.28	95.33	95.85
∠C13-As1-C12	97.59	99.10	99.09	97.09	97.14
∠C1-As1-C12	94.32	94.68	95.10	95.26	93.72
∠C6-O1-C7	123.04	124.44	123.65	123.21	123.36
∠*P*(C1C2C3C4C5C6)-*P*(C7C8C9C10C11C12)	20.84	14.22	17.29	17.32	17.39
∠*P*(C1C6C7C12)-*P*(C13C14C15C16C17C18)	93.96	86.56	84.20	84.28	84.87
∠O1-As1-C13-C14(C18*)	0.76	0.05	72.17*	58.20*	56.46*

Table S2. Selected interatomic distances (in Å) in **6**, **7**, and **10**.

	Complexes		
	6	**7**	**10**
Cu-Cu	Cu1-Cu1 2.787(2)	Cu1-Cu2 2.663(1)	Cu1-Cu1 2.683(1)
	Cu1-Cu1 2.811(2)	Cu1-Cu3 2.665(1)	Cu1-Cu1 2.782(1)
	Cu1-Cu1 2.811(2)	Cu1-Cu4 2.829(1)	Cu1-Cu1 2.782(1)
	Cu1-Cu1 2.811(2)	Cu2-Cu3 2.623(1)	Cu1-Cu1 2.782(1)
	Cu1-Cu1 2.811(2)	Cu2-Cu4 2.805(1)	Cu1-Cu1 2.782(1)
	Cu1-Cu1 2.787(2)	Cu3-Cu4 2.659(1)	Cu1-Cu1 2.683(1)
Cu-I	Cu1-I1 2.668(2)	Cu1-I1 2.6823(9)	Cu1-I1 2.6936(9)
	Cu1-I1 2.667(2)	Cu3-I1 2.6694(9)	Cu1-I1 2.6687(9)
	Cu1-I1 2.702(2)	Cu4-I1 2.660(1)	Cu1-I1 2.668(1)
	Cu1-I1 2.668(2)	Cu1-I2 2.708(1)	Cu1-I1 2.668(1)
	Cu1-I1 2.667(2)	Cu2-I2 2.6792(9)	Cu1-I1 2.6687(9)
	Cu1-I1 2.702(2)	Cu4-I2 2.6566(9)	Cu1-I1 2.6936(9)
	Cu1-I1 2.668(2)	Cu1-I3 2.6457(9)	Cu1-I1 2.668(1)
	Cu1-I1 2.667(2)	Cu2-I3 2.668(1)	Cu1-I1 2.6687(9)
	Cu1-I1 2.702(2)	Cu3-I3 2.6916(8)	Cu1-I1 2.6687(9)
	Cu1-I1 2.668(2)	Cu2-I4 2.7010(8)	Cu1-I1 2.668(1)
	Cu1-I1 2.667(2)	Cu3-I4 2.683(1)	Cu1-I1 2.6936(9)
	Cu1-I1 2.702(2)	Cu4-I4 2.665(1)	Cu1-I1 2.6936(9)
Cu-As	Cu1-As1 2.382(2)	Cu1-As4 2.355(1)	Cu1-As1 2.369(1)
	Cu1-As1 2.382(2)	Cu2-As3 2.348(1)	Cu1-As1 2.369(1)
	Cu1-As1 2.382(2)	Cu3-As1 2.338(1)	Cu1-As1 2.369(1)
	Cu1-As1 2.382(2)	Cu4-As2 2.363(1)	Cu1-As1 2.369(1)

Table S3. Selected structural parameters (distances in Å, angles in °) for **6**, **7**, and **10**.

	Complexes					
	6	**7***				**10**
As1…*P*(C1C6C7C12)/As2…*P*(C21C26C27C32)/ As3…*P*(C41C46C47C52)/As4…*P*(C61C66C67C72)	0.177	0.274	0.387	0.472	0.346	0.069
O1…*P*(C1C6C7C12)/O2…*P*(C21C26C27C32)/ O3…*P*(C41C46C47C52)/O4…*P*(C61C66C67C72)	0.114	0.155	0.223	0.316	0.224	0.108
As1…C13/As2…C33/As3…C53/As4…C73	1.980	1.935	1.943	1.940	1.943	1.945
∠C13-As1-C1/∠C33-As2-C21/ ∠C53-As3-C41/∠C73-As4-C61	97.97	102.72	101.17	100.74	102.70	103.05
∠C13-As1-C12/∠C33-As2-C32/ ∠C53-As3-C52/∠C73-As4-C72	98.72	103.30	102.45	104.74	100.18	105.32
∠C1-As1-C12/∠C21-As2-C32/ ∠C41-As3-C52/∠C61-As4-C72	97.05	97.18	95.13	94.58	96.01	96.85
∠C6-O1-C7/∠C26-O2-C27/ ∠C46-O3-C47/∠C66-O4-C67	125.27	123.66	123.89	121.55	122.48	124.62
∠*P*(C1-C6)-*P*(C7-C12)/∠*P*(C21-C26)-*P*(C27-C32)/ ∠*P*(C41-C46)-*P*(C47-C52)/ ∠*P*(C61-C66)-*P*(C67-C72)	1.23	14.26	18.87	29.16	19.44	10.30
∠*P*(C1C6C7C12)-*P*(C13-C18)/ ∠*P*(C21C26C27C32)-*P*(C33-C38)/ ∠*P*(C41C46C47C52)-*P*(C53-C58)/ ∠*P*(C61C66C67C72)-*P*(C73-C78)	0	72.46	88.01	84.44	87.82	89.96
∠O1-As1-C13-C14(C18)/∠O2-As2-C33-C34(C38)/ ∠O3-As3-C53-C54(C58)/∠O4-As4-C73-C74(C78)	13.73	35.76	47.14	26.26	40.20	5.40

* In **7**, four ligands have different geometries.

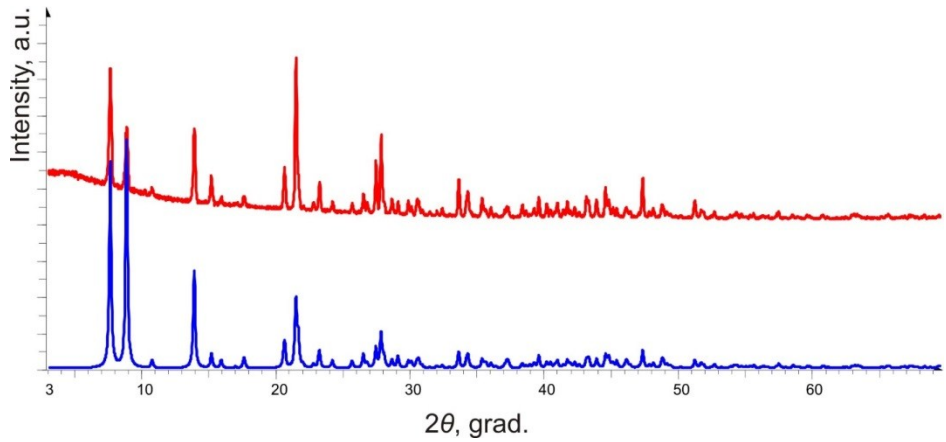

Figure S1. The theoretical powder diffractogram (blue line) calculated from the single crystal X-ray data for **6** and the experimental powder diffractogram (red line) of the dried polycrystalline powder sample.

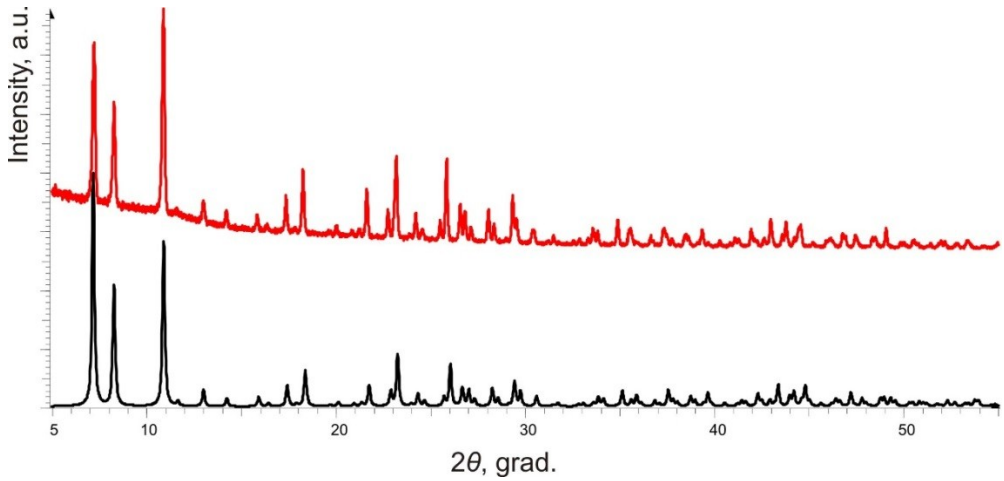

Figure S2. The theoretical powder diffractogram (black line) calculated from the single crystal X-ray data for **10** and the experimental powder diffractogram (red line) of the dried polycrystalline powder sample.

II. Photophysical properties

Experimental data:

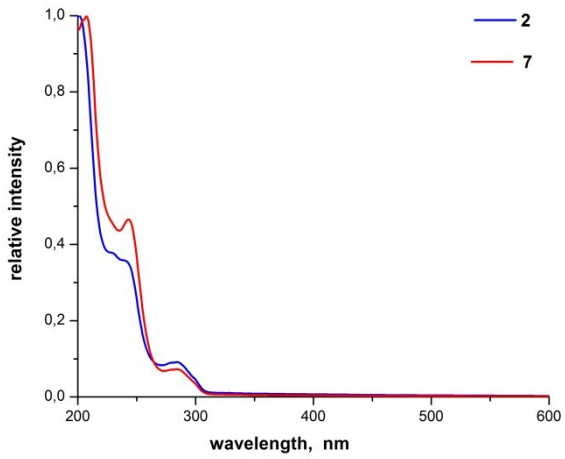

Figure S3. Experimental UV/Vis absorption spectra of the ligand **2** (c = $1.37 \cdot 10^{-5}$ mol·L^{-1}) and the corresponding complex **7** (c = $4.06 \cdot 10^{-6}$ mol·L^{-1}) recorded in acetonitrile solution. All measurements were recorded under ambient conditions.

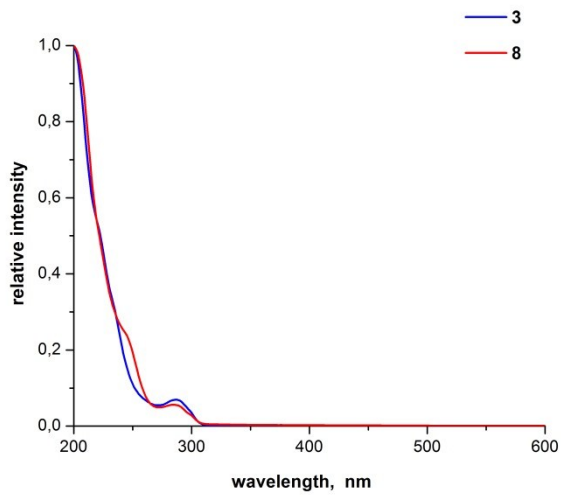

Figure S4. Experimental UV/Vis absorption spectra of the ligand **3** (c = $1.56 \cdot 10^{-5}$ mol·L^{-1}) and the corresponding complex **8** (c = $4.9 \cdot 10^{-6}$ mol·L^{-1}) recorded in acetonitrile solution. All measurements were recorded under ambient conditions.

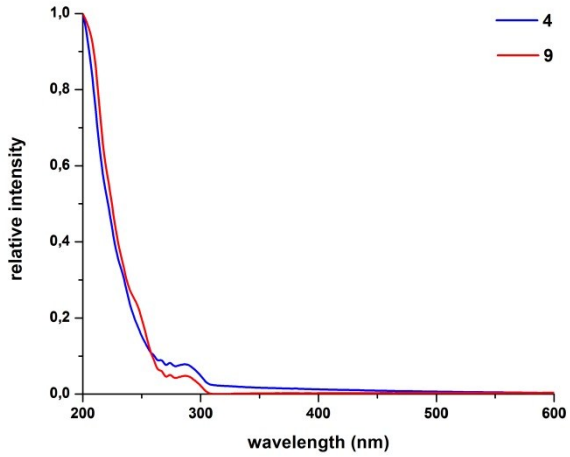

Figure S5. Experimental UV/Vis absorption spectra of the ligand **4** (c = $2.22 \cdot 10^{-5}$ mol·L^{-1}) and the corresponding complex **9** (c = $2.63 \cdot 10^{-6}$ mol·L^{-1}) recorded in acetonitrile solution. All measurements were recorded under ambient conditions.

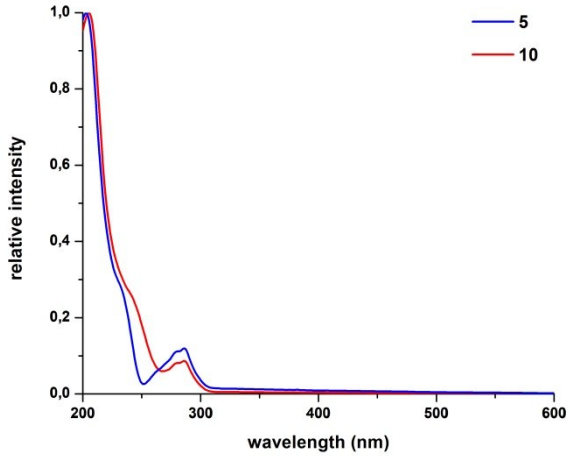

Figure S6. Experimental UV/Vis absorption spectra of the ligand **5** (c = $2.14 \cdot 10^{-5}$ mol·L^{-1}) and the corresponding complex **10** (c = $2.57 \cdot 10^{-6}$ mol·L^{-1}) recorded in acetonitrile solution. All measurements were recorded under ambient conditions.

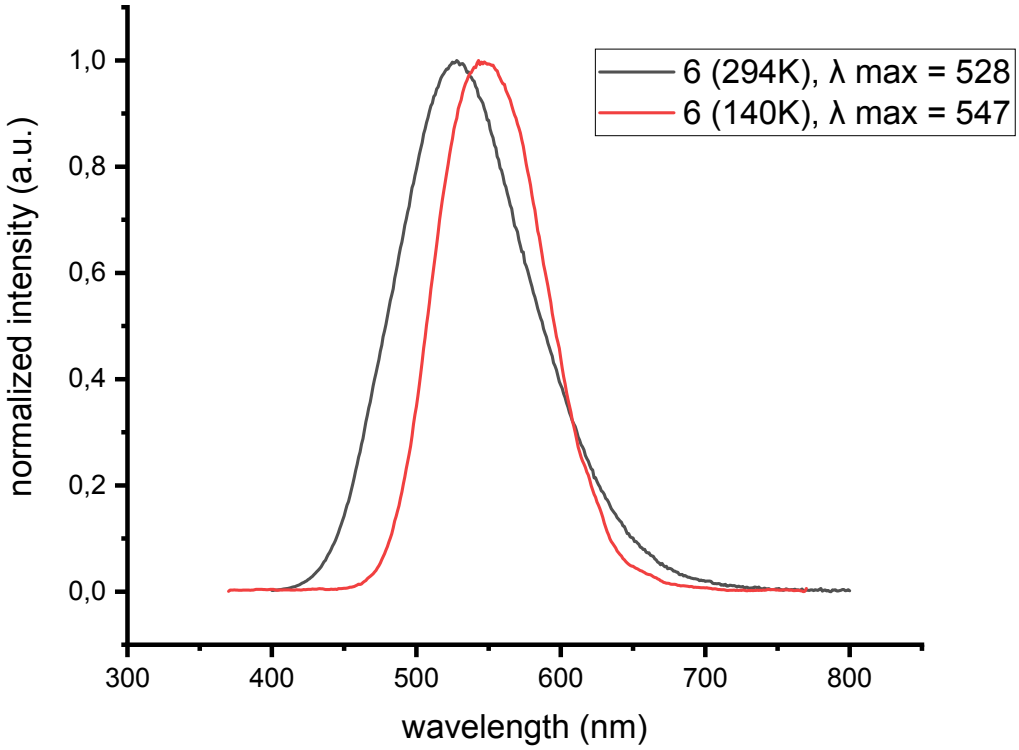

Figure S7. The solid-state emission spectra of complex **6** at 140 K and 294 K.

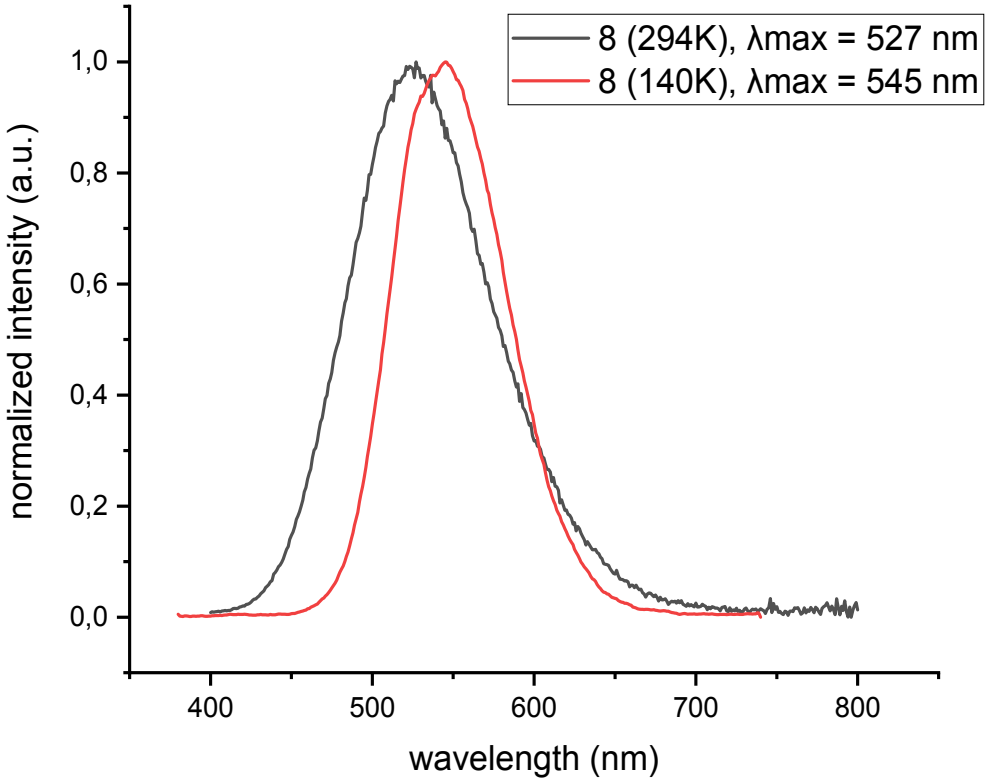

Figure S8. The solid-state emission spectra of complex **8** at 140 K and 294 K.

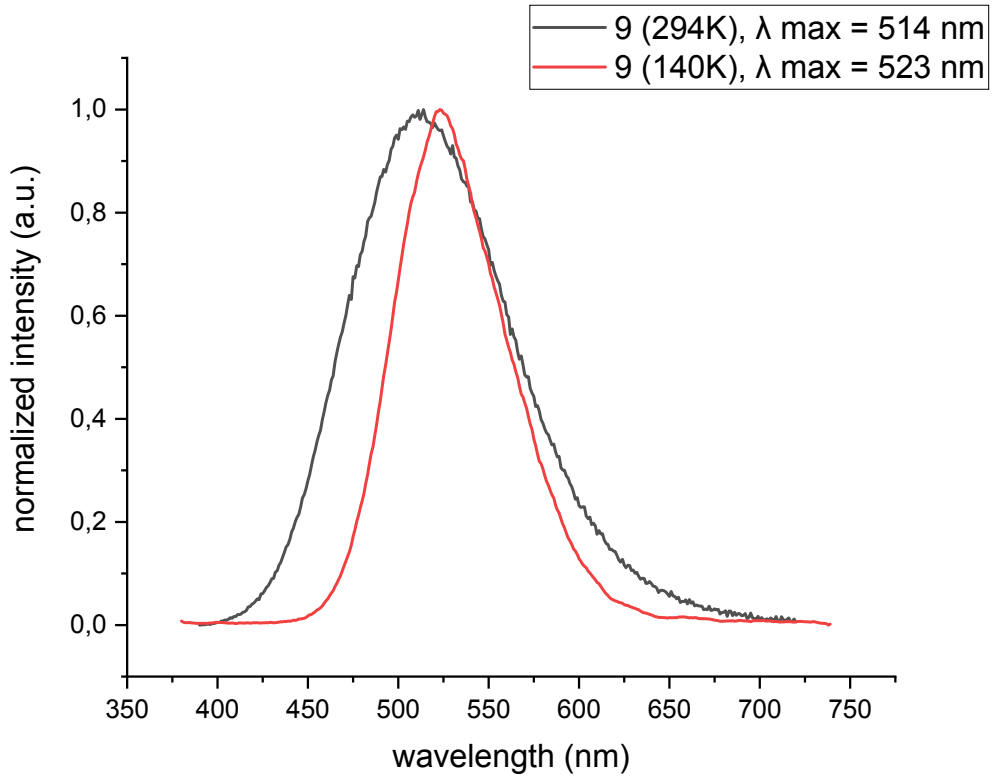

Figure S9. The solid-state emission spectra of complex **9** at 140 K and 294 K.

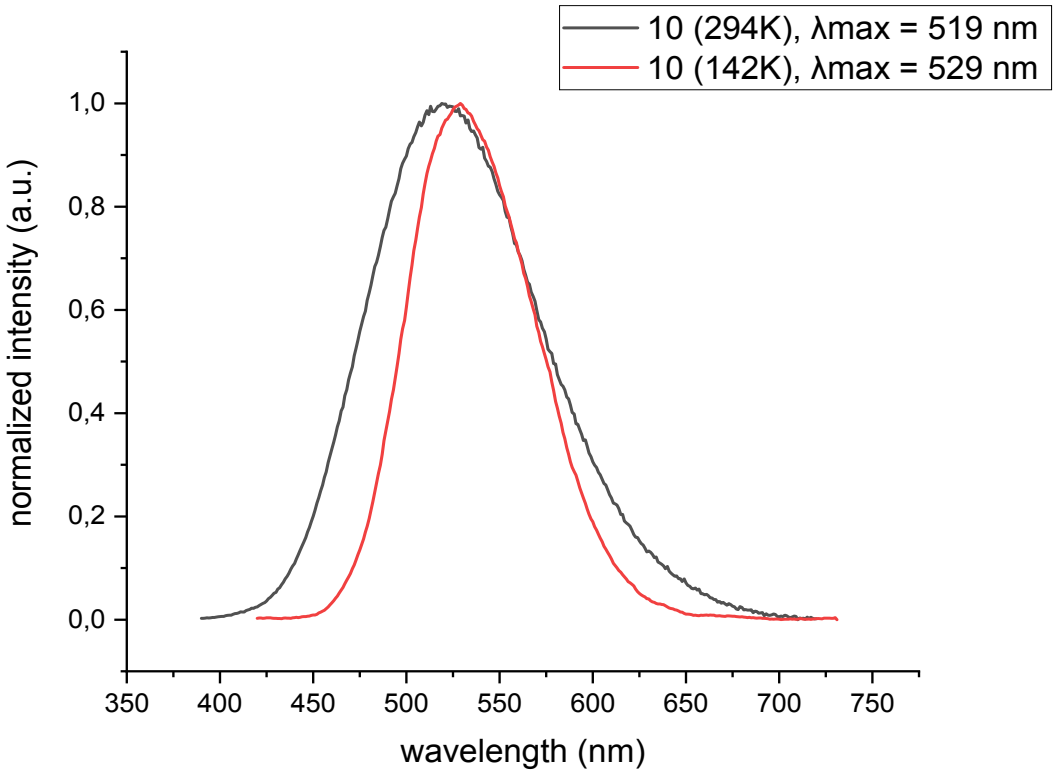

Figure S10. The solid-state emission spectra of complex **10** at 140 K and 294 K.

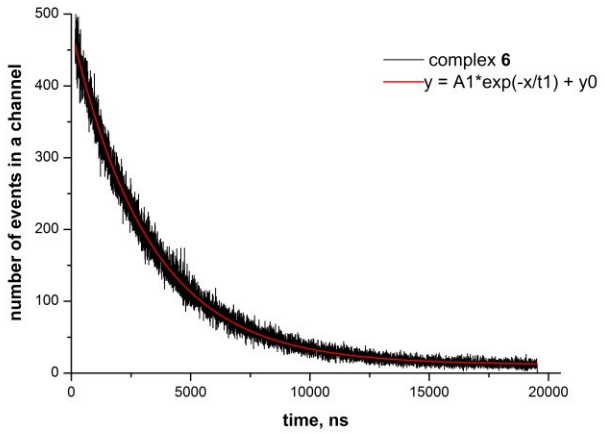

Figure S11. Trace of luminescence decay of complex **6**.

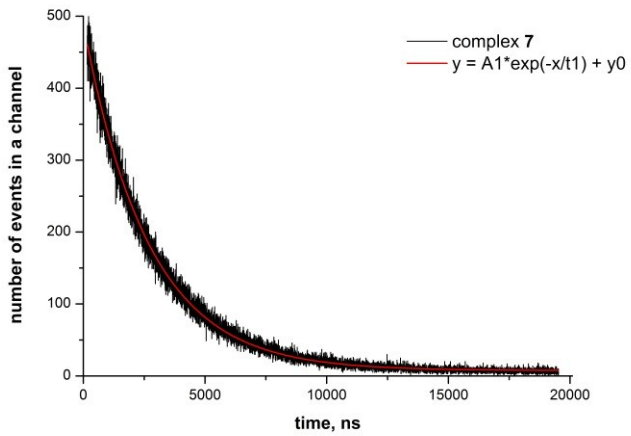

Figure S12. Trace of luminescence decay of complex **7**.

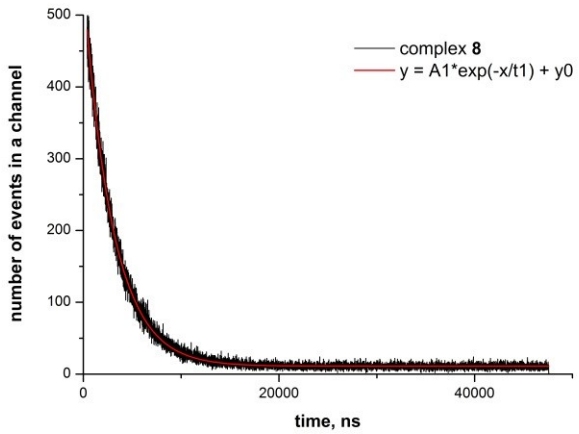

Figure S13. Trace of luminescence decay of complex **8**.

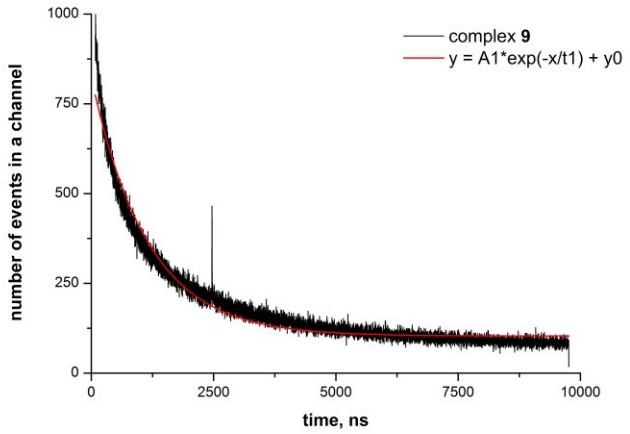

Figure S14. Trace of luminescence decay of complex **9**.

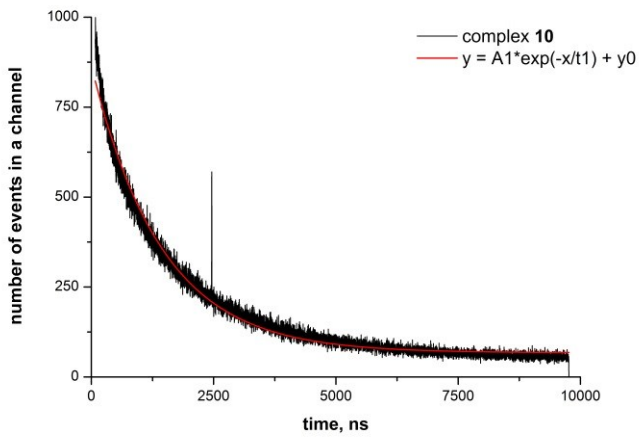

Figure S15. Trace of luminescence decay of complex **10**.

DFT-computed data for the ligands:

Figure S16 shows the UV/Vis solution spectra for ligands with para-substituted (**1** and **2**) and nonsubstituted (**3**) 10-aryl ring. In the case of bulky ethoxy substituent, the lowest-energy absorption band is slightly blue-shifted, and the spectrum has a pronounced shoulder. The peculiarities of the spectrum profile for the **2** solution compared to the **1** and **3** solutions were rationalized on the basis of our DFT-computed data.

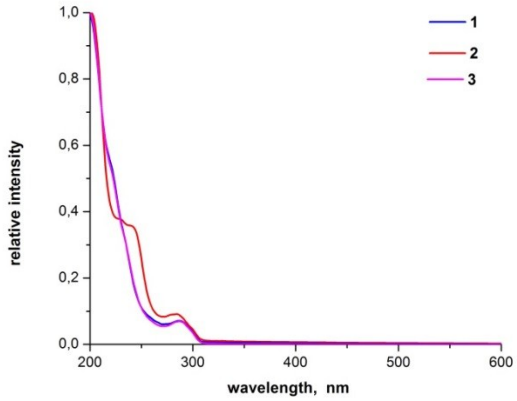

Figure S16. Experimental UV/Vis solution spectra for **1**–**3** (solvent – acetonitrile).

Since the X-ray data obtained for **1** and **3** indicate that the molecules of these ligands form supramolecular dimers in the solid state (Figure S17*a*), we considered both single molecules and supramolecular dimers. Along with the X-ray structure, Figure S8 shows the optimized structures of **1**-based supramolecular dimer, which were obtained with (*b*) and without (*c*) accounting for the influence of dispersion interactions. These structures can serve as models of a supramolecular dimer with strong and weak intermolecular interactions, respectively. Judging by the distances between the atoms of interacting molecules, the X-ray structure is intermediate between these two models, *i.e.*, intermolecular interactions are weakened in the solid state due to the crystal-packing effects. A more pronounced weakening of intermolecular interactions or even their absence one may expect in the solution due to the solvation effects.

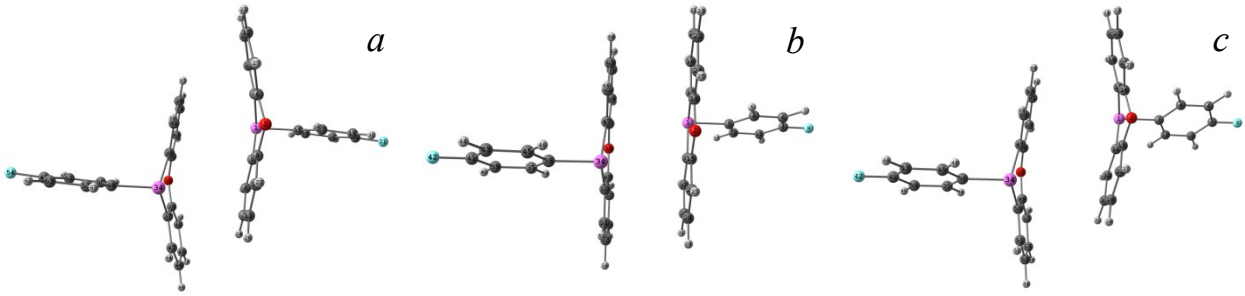

Figure S17. The **1**-based supramolecular dimer: crystal structure (*a*) and optimized structures obtained with (*b*) and without (*c*) accounting for the influence of dispersion interactions.

In the limiting case of strong intermolecular interactions (Figure S17*b*), the calculated absorption spectrum (Figure S18*a*) consists of low-energy, low-intensity electronic transitions in the wavelength range between 288 and 272 nm and high-energy electronic transitions giving rise to an intense peak at 225 nm and the most intense peak at 207 nm. The X-ray structure (Figure S17*a*) produces a similar spectrum. In the case of weak intermolecular interactions (Figure S17*c*), the spectrum profile is maintained, but the first absorption band is slightly blue-shifted from 288 to 279 nm (Figure S18*b*). Thus, a weakening of intermolecular interactions results in a blue shift of the lowest-energy absorption band. Note, however, that the spectrum is not very sensitive to the strength of dispersion interactions. One can see that the calculated data are in a good agreement with the UV/Vis solution spectrum: low-energy electronic transitions correspond to a weak absorption band at 287 nm and high-energy electronic transitions at ca. 225 nm – to a shoulder. In the absence of intermolecular interactions, the first absorption band is blue-shifted up to 269 nm (Figure S18*c*). One can see that the absorption spectrum calculated for this case is not consistent with experimental observations. Note that single molecules with and without dispersion interactions have similar geometric characteristics, and so they produce similar spectra. Thus, in the solution, the **1** molecules exist in the form of supramolecular dimers with relatively weak intermolecular interactions (of the same strength or weaker compared to the solid state). This conclusion applies to **3** as well.

The fact that the lowest-energy absorption band in the **2** case is slightly blue-shifted compared to the **1** and **3** solutions (Figure S16) indicates that, in the solution, the **2** molecules exist either in

the form of supramolecular dimers with even more weakened intermolecular interactions compared to **1**- and **3**-based supramolecular dimers or independently. From Figures S19 and S16, one can see that the agreement between the calculated and experimental data is observed only in the case of independent **2** molecule (Figure S19*c*): two low-energy electronic transitions at 278 and 273 nm correspond to the first absorption band in the experimental spectrum and high-energy electronic transitions in the wavelength range between 250 and 220 nm – to its shoulder. Thus, in the **2** case, the independent existence of solvated molecules is more preferable.

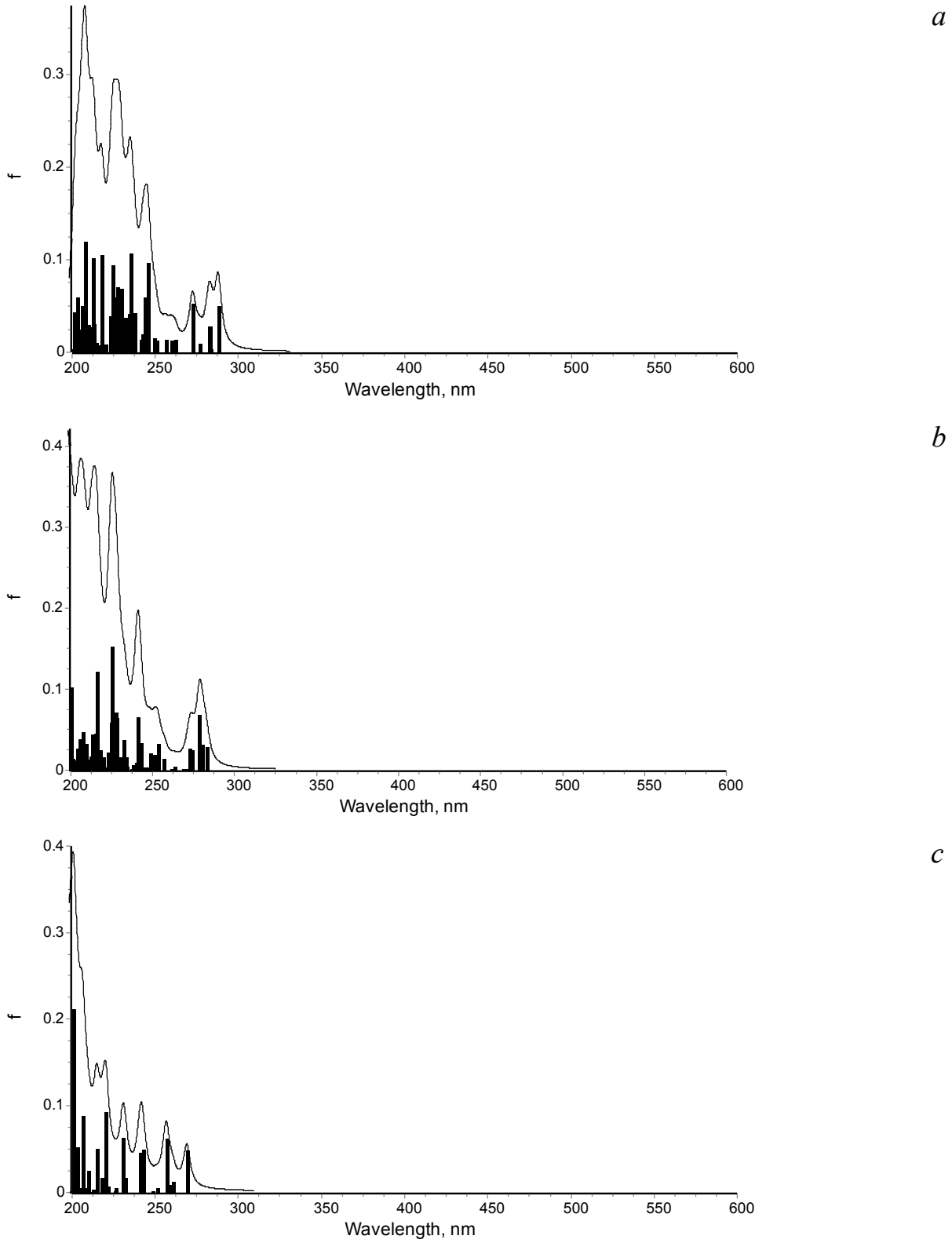

Figure S18. The calculated absorption spectra for (*a*, *b*) **1**-based supramolecular dimer with strong and weak intermolecular interactions and (*c*) independent **1** molecule. The vertical lines showing the position of singlet-singlet electronic transitions and their intensity (*f* – oscillator strength) were broadened by the Lorentz function (f.w.h.m. = 0.25 eV).

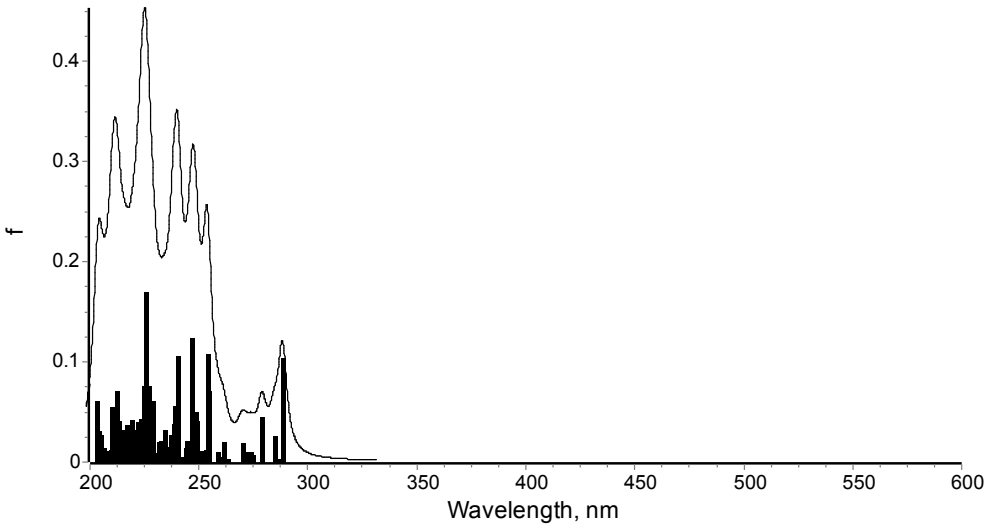

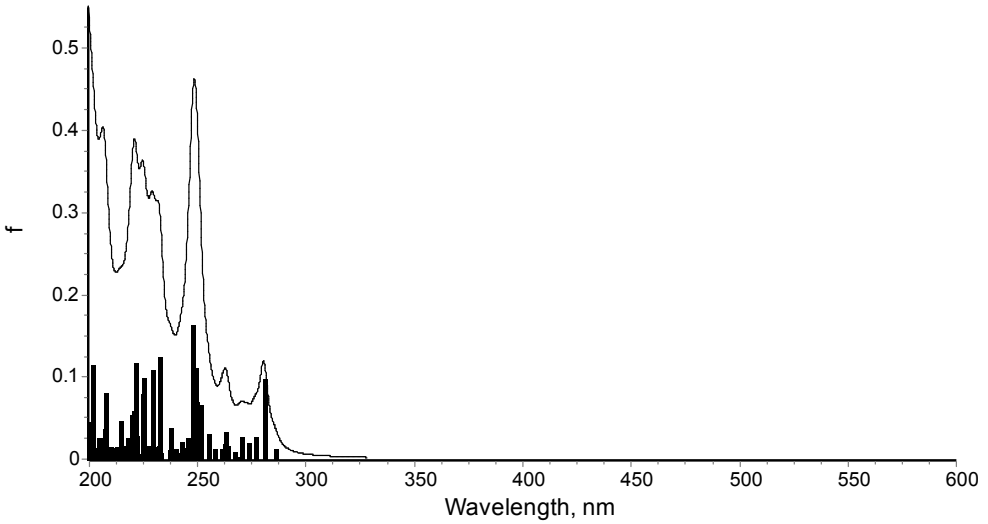

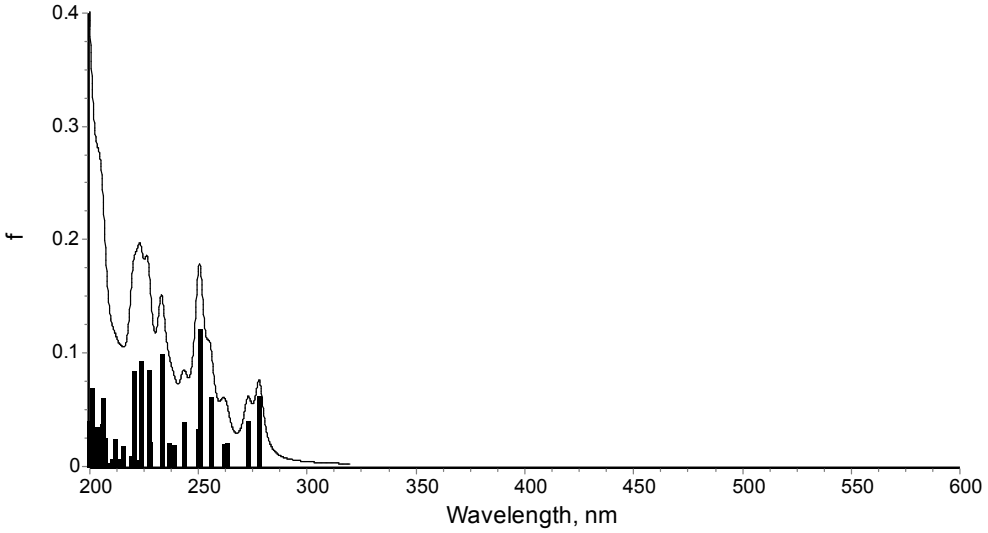

Figure S19. The calculated absorption spectra for (*a*, *b*) **2**-based supramolecular dimer with strong and weak intermolecular interactions and (*c*) independent **2** molecule. The vertical lines showing the position of singlet-singlet electronic transitions and their intensity (*f* – oscillator strength) were broadened by the Lorentz function (f.w.h.m. = 0.25 eV).

DFT-computed data for the complexes:

Table S4. Selected equilibrium singlet ground-state structural parameters (distances in Å) for **6** and [Cu_4I_4(pyridine)$_4$] obtained within the framework of different computational procedures.

	Cu…Cu	Cu–I
(*a*) **6**: C_1 symmetry (S_4 in parentheses)		
X-ray data	(2.787–2.811)	(2.667–2.702)
PBE0/LANL2DZ	2.801–2.814	2.753–2.761
	(2.790–2.841)	(2.750–2.764)
B3LYP/LANL2DZ	2.963–3.030	2.784–2.812
	(2.947–3.000)	(2.792–2.802)
PBE0/def2-TZVP	2.793–2.933	2.690–2.745
PBE0-D3(BJ)/def2-TZVP	2.645–2.718	2.655–2.763
B3LYP-D3(BJ)/def2-TZVP	2.647–2.722	2.685–2.814
(*b*) [Cu_4I_4(pyridine)$_4$]: D_{2d} symmetry		
X-ray data[a]	2.619–2.722	2.665–2.734
PBE0/LANL2DZ	2.661–2.783	2.771–2.802
B3LYP/LANL2DZ[b]	2.685–2.834	2.817–2.861

[a] C. L. Raston, A. H. White, *J. Chem. Soc., Dalton Trans.*, 1976, 2153-2156; [b] F. De Angelis, S. Fantacci, A. Sgamellotti, E. Cariati, R. Ugo, P. C. Ford, *Inorg. Chem.*, 2006, **45**, 10576-10584.

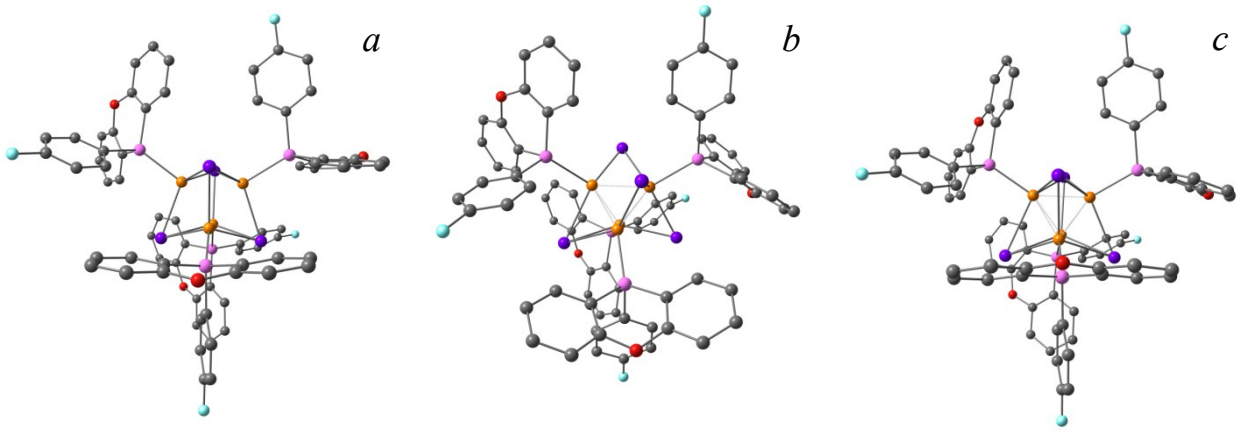

Figure S20. The optimized structures for the singlet ground state S_0 (*a*) and the lowest triplet state T_1 obtained without (*b*) and with (*c*) accounting for the molecular symmetry found in the X-ray structure (complex **6**).

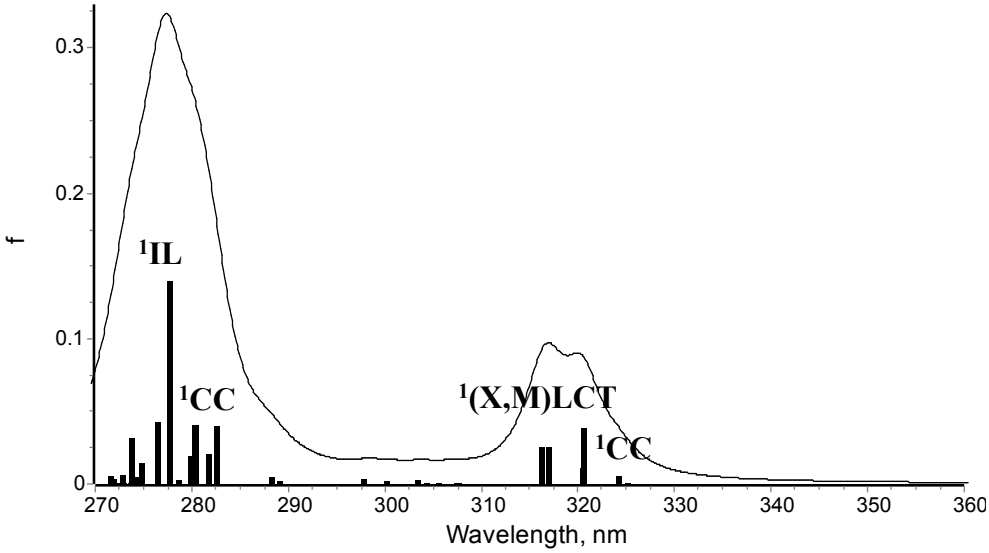

Figure S21. The calculated absorption spectra for **6**. The vertical lines showing the position of singlet-singlet electronic transitions and their intensity (*f* – oscillator strength) were broadened by the Lorentz function (f.w.h.m. = 0.25 eV).

Table S5. The calculated excitation energies (absorption wavelengths), oscillator strengths, natural transition orbital (NTO) pairs and their eigenvalues (occupations) for selected excited states of **6**.

subset: type	λ	f	№	occ.	NTO pair	
I: ^{1}CC	325	0.00	1	0.98	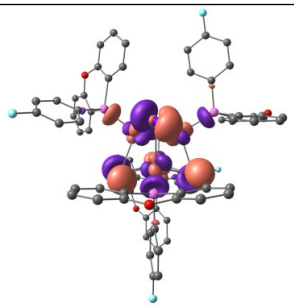 HOMO	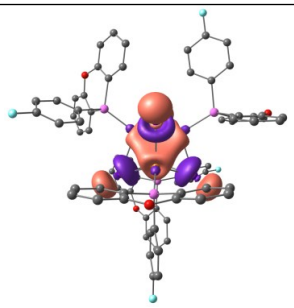 LUMO+8
	324	0.01	2	0.98	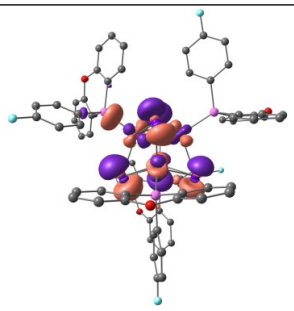 HOMO–1	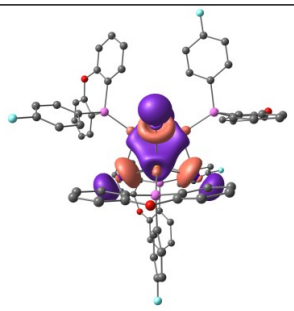 LUMO+8
	324	0.01	3	0.98	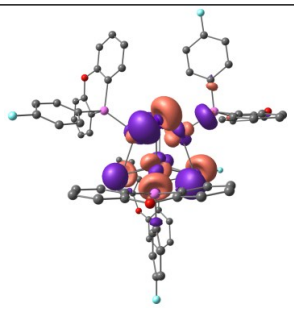 HOMO–2	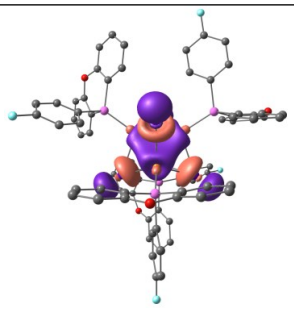 LUMO+8
II: ^{1}(X,M)LCT	321	0.04	4	0.61 0.23 0.15	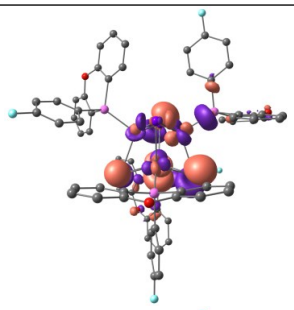 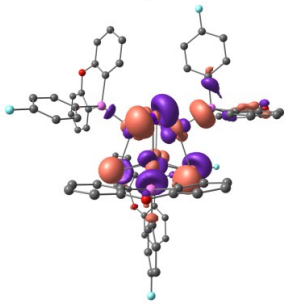	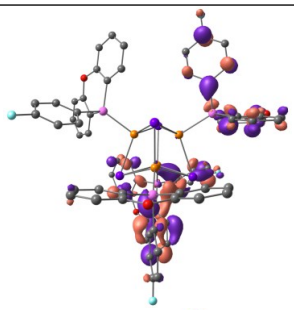 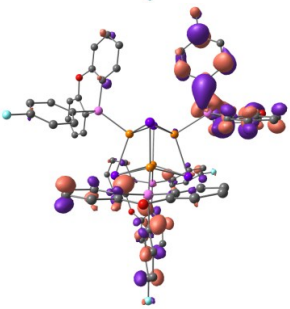

					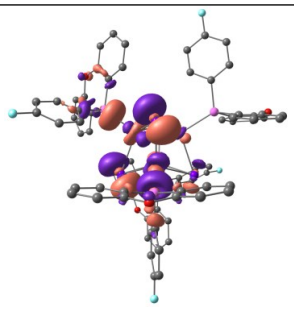	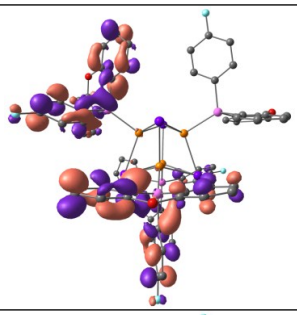
	317	0.03	8	0.43 0.30 0.26	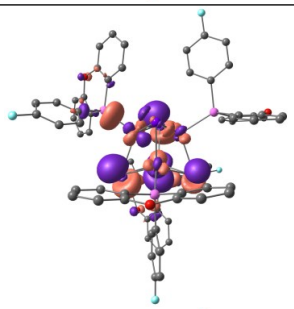 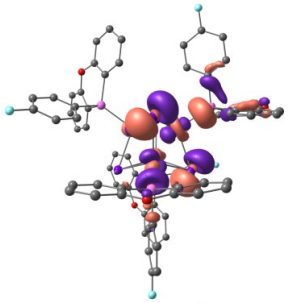 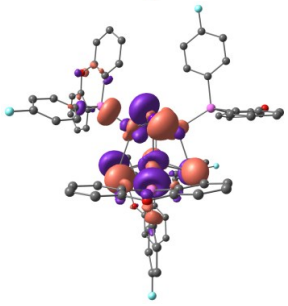	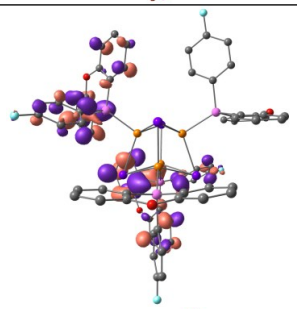 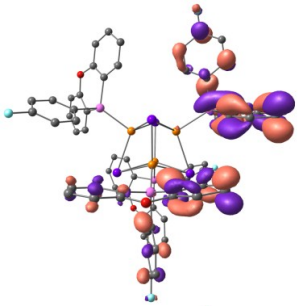 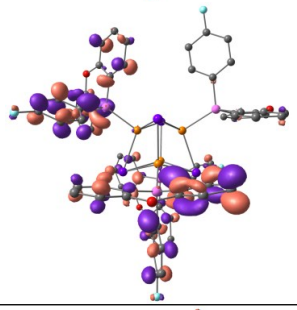
	317	0.03	9	0.42 0.30	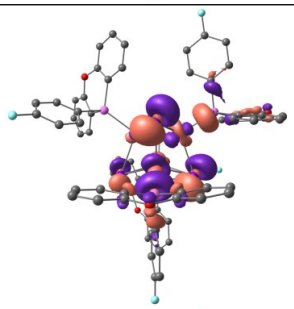 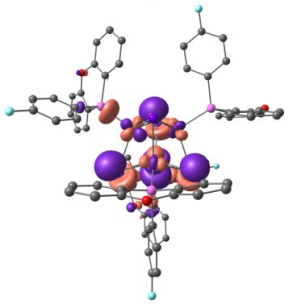	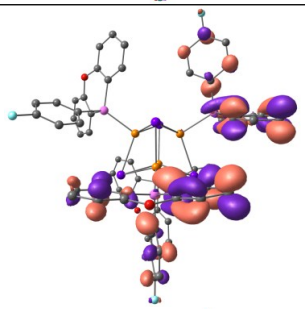 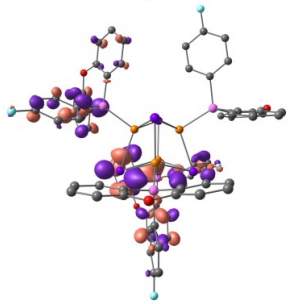

				0.26	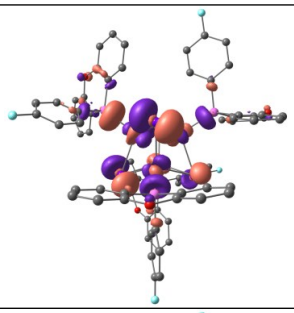	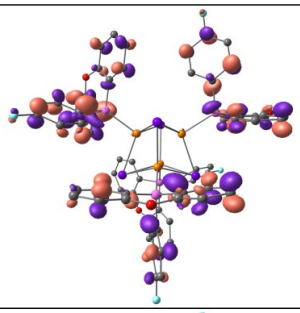
	316	0.02	10	0.46	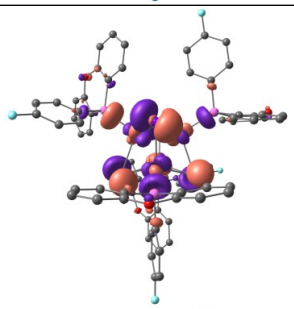	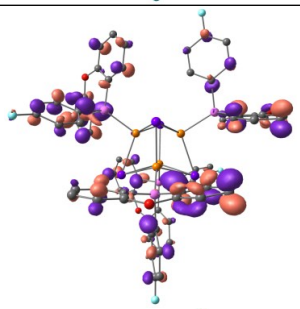
				0.27	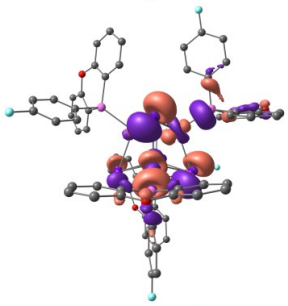	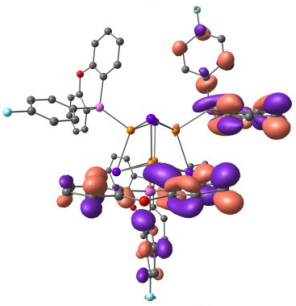
				0.26	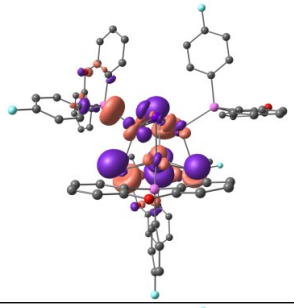	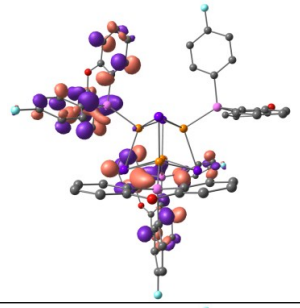
III: ^{1}CC with a small admixture of ^{1}(X,M)LCT	282	0.04	43	0.74	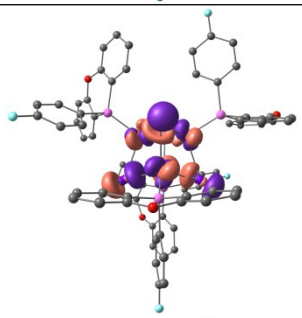	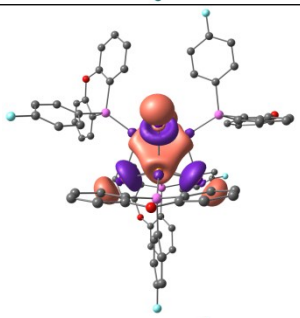
				0.13	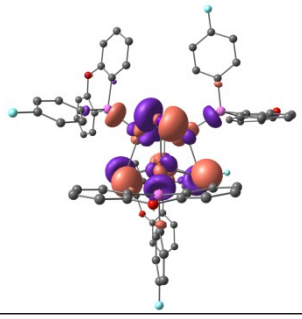	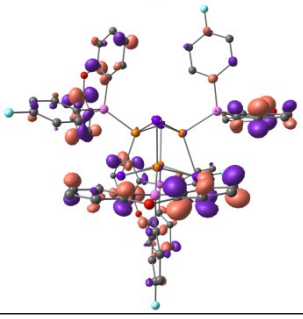

	280	0.04	47	0.62 0.20	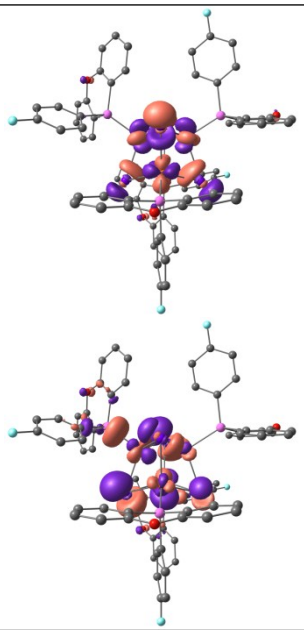	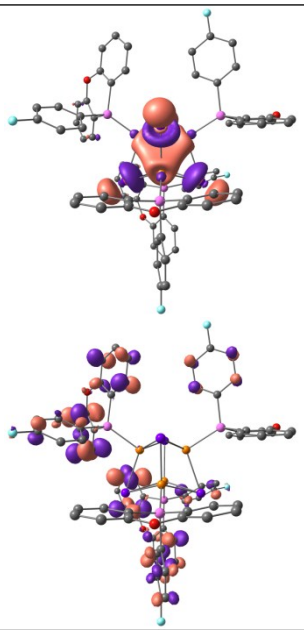
	280	0.04	48	0.62 0.20	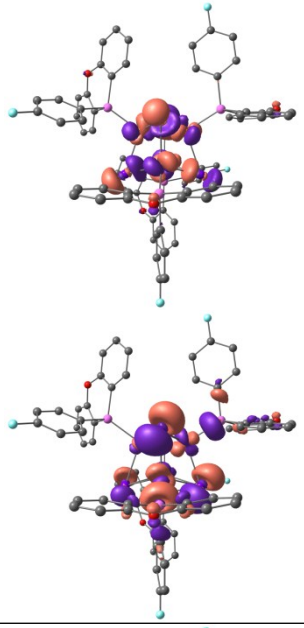	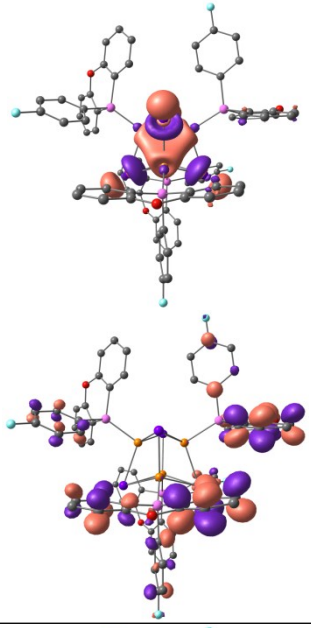
IV: ^{1}IL with a small admixture of ^{1}(X,M)LCT	278	0.14	52	0.25 0.23	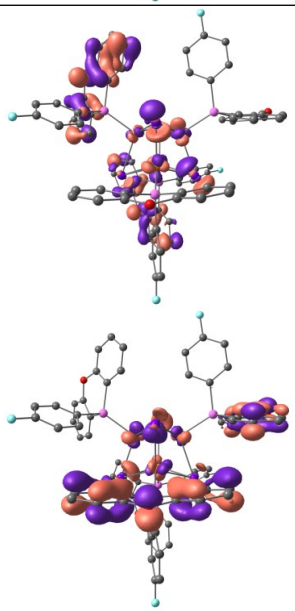	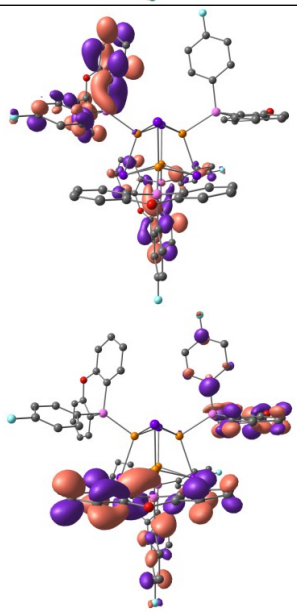

				0.19 0.16	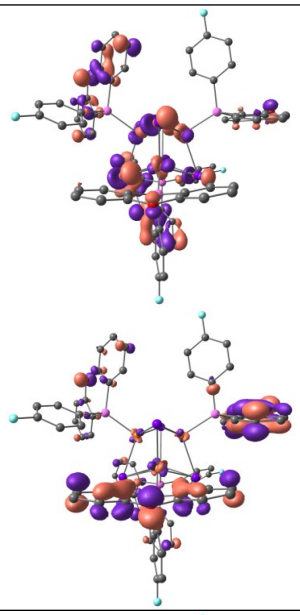	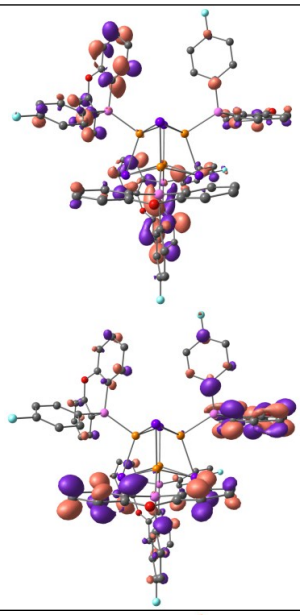
	276	0.04	54	0.55 0.17	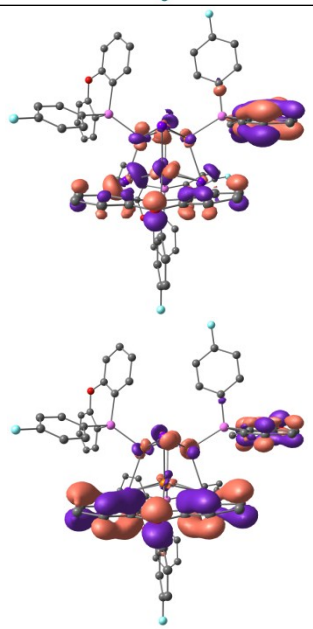	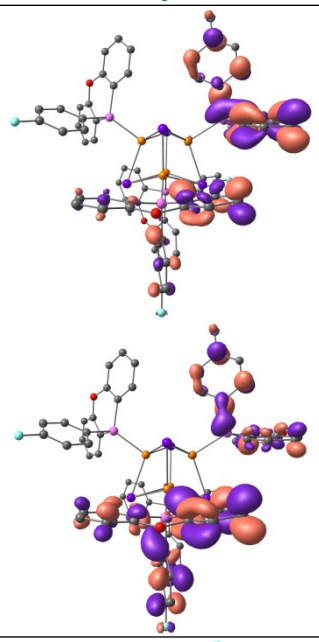
	276	0.04	55	0.55 0.18	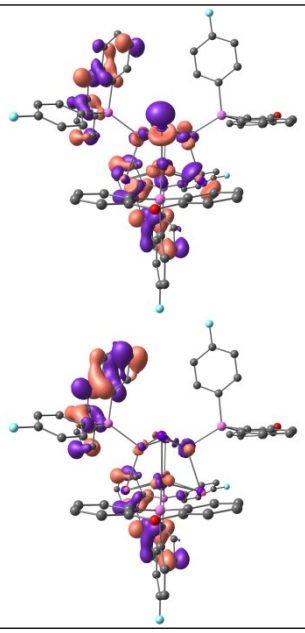	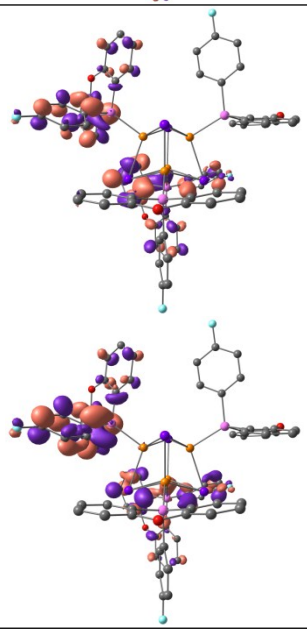

III. A collection of the solid-state phosphorescence emission maxima data for different Cu_4I_4 cubanes at room temperature

donor atom	Compound	λ_{em}, nm		Cu…Cu	Ref.
		LE	HE		
N	$[Cu_4I_4(pyridine)_4]$	580 570		 <2.690>	[13] [15]
	$[Cu_4I_4(1\text{-methylimidazole})_4]$	636		2.636–2.865	[16]
	$[Cu_4I_4(1,1'\text{-methylene-bis(imidazole)})_2]_\infty$	600 645		2.634–2.750 2.646–2.721	[16]
	$[Cu_4I_4(piperidine)_4]$	570 581		2.595–2.640 <2.643> <2.657>	[15] [19]
	$[Cu_4I_4(N\text{-methyl-piperidine})_4]$	560		2.868–2.946	[15]
	$[Cu_4I_4(quinuclidine)_4]$	540		2.671–2.696	[15]
	$[Cu_4I_4(3\text{-quinuclidinol})_4]$	550 565		2.695–2.720 <2.688>	[15]
P	$[Cu_4I_4(PPh_2(CH_2CH{=}CH_2))_4]$	515 530		<3.249> 3.179–3.390	[18] [19]
	$[Cu_4I_4(PPh_2(CH_2CH_2CH_3))_4]$	565 560		<3.14> <3.14>	[18] [20]
	$[Cu_4I_4(PPh_2(OCH_2CH_3))_4]$	570 580		<3.056> <2.871>	[21]
	$[Cu_4I_4(Pcpent_3)_4]$	523		<3.276>	[20]
	$[Cu_4I_4(PPh_3)_4]$	545		<2.901>	[20]
	$[Cu_4I_4(P(C_6H_4{-}OCH_3)_3)_4]$	558		<3.126>	[22]
	$[Cu_4I_4(P(C_6H_4{-}CH_3)_3)_4]$	515		<3.007>	[22]
	$[Cu_4I_4(P(C_6H_4{-}CF_3)_3)_4]$	525	440	<2.953>	[22]
	$[Cu_4I_4(P(m\text{-Anisyl})_3)_4]$	545		3.127–3.268	[23]
	$[Cu_4I_4(P(p\text{-Anisyl})_3)_4]$	540		2.790–3.309	[23]
As	**6**	528		<2.803>	
	7	534		<2.707>	
	10	520		<2.749>	
Sb	$[Cu_4I_4(Sb^tBu_3)_4]^a$	558		<2.975>	[27]
	$[Cu_4I_4(SbCy_3)_4]^a$	666		<2.826>	[27]
	$[Cu_4I_4(Sb^tBu_2Ph)_4]^a$	575		<2.822>	[27]
	$[Cu_4I_4(Sb^iPr_3)_4]^a$	711		<2.761>	[27]

[a] The data were obtained at 77 K.